TITLE PAGE

Experimental colitis drives enteric alpha-synuclein accumulation and Parkinson-like brain pathology

Stefan Grathwohl[1], Emmanuel Quansah[2], Nazia Maroof[1], Jennifer A. Steiner[2], Liz Spycher[1], Fethallah Benmansour[3], Gonzalo Duran-Pacheco[4], Juliane Siebourg-Polster[4], Krisztina Oroszlan-Szovik[1], Helga Remy[1], Markus Haenggi[1], Marc Stawiski[1], Matthias Sehlhausen[4], Pierre Maliver[4], Andreas Wolfert[5], Thomas Emrich[5], Zachary Madaj[2], Martha L. Escobar Galvis[2], Christoph Mueller[6], Annika Herrmann[4], Patrik Brundin[2], and Markus Britschgi[1]

[1] Roche Pharma Research and Early Development, Neuroscience Discovery, Roche Innovation Center Basel, F. Hoffmann-La Roche Ltd, Grenzacherstrasse 124, Basel, Switzerland

[2] Center for Neurodegenerative Science, Van Andel Research Institute, 333 Bostwick Ave. NE, Grand Rapids, MI, USA

[3] Roche Pharma Research and Early Development, pREDi, Roche Innovation Center Basel, F. Hoffmann-La Roche Ltd, Grenzacherstrasse 124, Basel, Switzerland

[4] Roche Pharma Research and Early Development, Pharmaceutical Sciences, Roche Innovation Center Basel, F. Hoffmann-La Roche Ltd, Grenzacherstrasse 124, Basel, Switzerland

[5] Roche Pharma Research and Early Development, Pharmaceutical Sciences, Roche Innovation Center Munich, Roche Diagnostics GmbH, Nonnenwald 2, 82377 Penzberg, Germany

[6] Institute of Pathology, University of Bern, Murtenstrasse 31, Bern, Switzerland

Corresponding authors:

Markus Britschgi, Roche Pharma Research and Early Development, Neuroscience Discovery, Roche Innovation Center Basel, F. Hoffmann-La Roche Ltd, Grenzacherstrasse 124, Basel, Switzerland

Tel: +41 61 6879116

Email: markus.britschgi@roche.com

Patrik Brundin, Van Andel Research Institute, 333 Bostwick Ave. NE, Grand Rapids, MI 49503, USA.

Tel: +1 616.234.5312

Email: patrik.brundin@vai.org

Abstract

Intraneuronal accumulation of α-synuclein (αSyn) is key in the pathogenesis of Parkinson's disease (PD). Published studies suggest that this process begins in the enteric nervous system (ENS) and propagates into the brain decades before clinical diagnosis of PD. The triggers and mechanisms underlying the accumulation of αSyn remain unknown but evidence is growing that immune pathways and in particular colitis may play a critical role. Here we demonstrate that patients with inflammatory bowel disease (IBD) exhibit αSyn accumulation in their colon. We then confirmed in an experimental model of IBD that intestinal inflammation can trigger αSyn accumulation in the ENS of wildtype and αSyn transgenic mice. We discovered that the type and degree of inflammation modulates the extent of αSyn accumulation in the colon and that macrophage-related signaling limits this process. Remarkably, experimental colitis at three months of age exacerbated the accumulation of aggregated phospho-Serine 129 αSyn in the midbrain, including the substantia nigra, in 21-month but not 9-month-old αSyn transgenic mice. This was accompanied by loss of nigral tyrosine hydroxylase-immunoreactive neurons, another neuropathological hallmark of PD. Together, our data suggest a critical role for intestinal inflammation in the initiation and progression of PD.

Introduction

Parkinson's disease (PD) is a progressively debilitating neurodegenerative disease affecting 1% of the population above 60 years (1). Typical symptoms are motor impairments including muscle rigidity, tremor, and bradykinesia. Neuropathologically, PD is hallmarked by dopaminergic cell loss in the substantia nigra (SN), a resultant loss of striatal dopaminergic signaling (2, 3), and the presence of intraneuronal inclusions called Lewy bodies and neurites (4, 5). Lewy pathology is enriched in α-synuclein (αSyn), a presynaptic protein that tends to misfold, aggregate, and become phosphorylated under pathological conditions (2, 3). Alpha-synuclein is also genetically linked to rare familial forms of PD and certain SNPs close to the αSyn gene (*SNCA*) locus are associated with an increased risk for developing PD (6). These findings in humans make αSyn a focal point of biomarker and drug development programs for PD.

Several years before the first appearance of motor features, many patients exhibit a variety of non-motor symptoms including constipation, sleep disorder, depression, and hyposmia (7–9). Co-occurrence of some of these non-motor symptoms increases the risk of progressing to PD even in otherwise healthy individuals in population-based and cohort studies (10–13). Constipation may be a particularly important non-motor feature of preclinical PD, with 28-61% of patients often exhibiting gastrointestinal dysfunction years before progressing to motor symptoms (9, 12, 14). This suggests an early connection between the status of the intestinal environment and the progression to PD (15). In line with this connection and due to the discovery of αSyn immunoreactive inclusions in neurons of the submucosal plexus in people with PD, Braak and colleagues have suggested an early involvement of the enteric nervous system (ENS) in the pathogenesis of PD (4, 5, 16, 17). It is currently unclear whether occurrence of αSyn aggregates in the peripheral nervous system is specific for PD since individuals with dementia with Lewy bodies and normal people can also show such inclusions in various tissues (18–21). Yet based on their findings, Braak and colleagues hypothesized that αSyn immunoreactive inclusions first appear in the ENS and then progress over time to the brainstem regions, including the dorsal motor nucleus of the vagus nerve and midbrain areas (4, 5, 16, 17). Several studies in preclinical models have recently demonstrated a potential propagation of αSyn

pathology in the gut and the brain (22–26). Intriguingly, a clinical study reported that vagotomy in a Danish population decreases the risk of PD (27). Determining the critical factors for αSyn pathology in the ENS could provide insights into disease etiology, enabling the development of novel treatment paradigms to slow disease progression. A key factor that could trigger ENS αSyn accumulation and pathology spread is inflammation.

Interestingly, a recent finding in children with gastrointestinal inflammation suggests an immune regulatory function of αSyn (28). Immune pathways are indeed activated in the brain and colon of PD cases (29, 30). Also, several genes associated with an increased risk of developing PD have an immune system-related function (31), and a recent genome-wide association study identified common genetic pathways linking PD and autoimmune disorders (32). Most prominently, LRRK2, a major genetic risk factor for PD also confers increased risk for developing inflammatory bowel disease (IBD) (33) and is known to modulate the function of monocytes, macrophages and other immune cells (34, 35). Intriguingly, IBD is now confirmed to be associated with an increased risk for developing PD and specifically blocking the TNF pathway reduces this risk (36–38).

Here we tested the hypothesis that intestinal inflammation (e.g. colitis) triggers αSyn aggregation in the ENS and the subsequent development of αSyn pathology in the brain. We discovered that patients with IBD exhibited increased αSyn accumulation in the submucosal region of the colon. Experimental colitis in wild type and αSyn transgenic mice demonstrated that the type and degree of inflammation modulates the extent of αSyn accumulation in the colon and that macrophage-related signaling limits this process. Remarkably, experimental colitis at 3 months of age exacerbated the accumulation of aggregated αSyn in midbrain, including the SN, in 21-month but not 9-month-old αSyn transgenic mice. This was accompanied by loss of nigral tyrosine hydroxylase-immunoreactive neurons. Together, our data suggest a critical role for intestinal inflammation in the initiation and progression of PD.

Results

IBD patients show αSyn accumulation in the ENS and local macrophages

Recent epidemiological data links inflammatory bowel disease (IBD) to an increased risk of developing PD (36–38). In order to explore if IBD is associated with enteric αSyn accumulation we performed immunohistochemistry for αSyn in cryo-sections from colonic biopsies of patients with ulcerative colitis (UC, n = 11, mean age 31 years), Crohn's disease (CD, n = 11; mean age 35 years), and from healthy subjects (HS, n = 8; mean age 51 years). We observed in eight UC cases various degrees of αSyn accumulation, mostly in neuritic structures (**Figure 1**). Interestingly, the eight UC cases, and four patients with CD (images not shown) also showed marked intracellular αSyn staining in many infiltrating monocytic cells. In contrast, only one HS showed a few immunoreactive cells (images not shown). This finding in human tissue suggests a potential role of local inflammation in the development of enteric αSyn accumulation.

Experimental IBD exacerbates αSyn load in submucosal plexus of αSyn transgenic and wildtype mice

During the process of further characterizing a (Thy1)-h[A30P]αSyn transgenic mouse line (39) we detected human αSyn accumulation in all innervated organs that were analyzed (**Supplemental Figure 1**). This included the myenteric and submucosal plexuses of the ENS, where it co-localized with peripherin, a specific marker for peripheral nerves (**Figure 2A).** We observed an age-dependent increase of baseline αSyn inclusion in both plexuses between the age of three and twelve months (**Figure 2B**). Since this transgenic model has the capacity to increase the αSyn load in the ENS over several months we wanted to test the hypothesis whether IBD-related inflammation in the colon may trigger or exacerbate local αSyn accumulation more acutely, e.g. within a few days or weeks. Administration of dextran sulfate sodium (DSS) in the drinking water in acute or chronic paradigms is a well-established mouse model of IBD colitis, resulting in infiltration of leukocytes into the submucosa with various degrees of destruction of the colonic tissue and the mucosa (40). We administered DSS at different concentrations and durations to (Thy1)-h[A30P]αSyn transgenic mice (**Figure 2C**), resulting in leukocyte infiltration in a dose-dependent manner (**Figure 2D and 3A**).

Intriguingly, in the acute paradigm, 2.5% but not 1% DSS triggered intracellular accumulation of αSyn in the submucosal plexus **(Figure 3A, B)**. In the chronic DSS paradigm, a dose-dependent increase of αSyn load in the submucosal plexus was observed **(Figure 3A)**. To confirm that this finding was independent of transgenic expression of human αSyn, acute and chronic (consistent dose) DSS paradigms were respectively applied also in wildtype mice. In both paradigms, we observed aggregation of endogenous murine αSyn in the submucosal plexus **(Figure 3C, D)**. A separate experiment also confirmed that the observed effects of DSS could not be attributed to increased gene expression of murine or the transgenic human αSyn **(Supplemental Figure 2)**. Together, these results confirmed the validity of this experimental IBD paradigm to test the effect of inflammation on αSyn accumulation in the ENS.

Colitis induced by peroral DSS but not by peritoneal administration of LPS aggravates αSyn accumulation in colonic submucosal plexus of αSyn transgenic mice

In order to explore effects of different approaches to induce inflammation in or nearby the gut in (Thy1)-h[A30P]αSyn transgenic mice, we compared the outcome of an acute 5% DSS in drinking water with acute intraperitoneal LPS administration (**Figure 2C and 4**). At d7, both agents had induced variable degrees of leukocyte infiltration in the submucosa of the colon with a marked destruction of the mucosa induced by only DSS (**Figure 2D**). As before, the DSS-exposed mice presented with increased mean accumulation of αSyn in the ganglia of the submucosal plexus (**Figure 4A**). In contrast, no change in αSyn load was detected in the myenteric plexus, consistent with lack of leukocyte infiltration in this anatomical region of the colon (**Figure 4B**). Interestingly, LPS-induced inflammation did not increase αSyn accumulation in the colonic nervous plexuses (**Figure 4C, D**). The two inflammatory insults resulted, however, in a differential expression of cytokines, and consistent with leukocyte recruitment, CCL2 was elevated in both (**Figure 4F, G**). Interestingly, in the LPS paradigm, mRNA for IL-10 was markedly elevated, whereas DSS strongly increased IL-6 and also IL-1β but not IL-10. Together these results indicate that certain types of local inflammation can increase the intracellular accumulation of aggregated αSyn in the periphery (i.e. in the colon).

157 ***Lack of Cx3cr1 signaling during DSS colitis aggravates αSyn load in the submucosal plexus of***
158 ***αSyn transgenic mice***

159 In both the IBD patients as well as the (Thy1)-h[A30P]αSyn transgenic mice that experienced acute
160 DSS colitis, we observed by their morphology αSyn positive infiltrating cells (**Figure 5)**. In the mice
161 these infiltrating cells were positive for the macrophage marker Iba-1 (**Figure 5C-D**). In order to
162 explore further the role of monocytes/macrophages in the accumulation of αSyn in our DSS model,
163 we added an experimental arm with (Thy1)-h[A30P]αSyn transgenic mice crossed with mice that
164 have a deletion of Cx3cr1 induced by an insertion of GFP (Cx3cr1-GFP knock-in mice) (**Figure 4A,**
165 **B**). The CX3CR1-CX3CL1 axis plays an important role in maintaining the function of the lamina
166 propria macrophage population of the gastrointestinal wall and lack of this signaling pathway in
167 experimental colitis models may either aggravate or ameliorate the induced pathology (41–43). In our
168 experiment exposure to DSS resulted in leukocyte infiltration in the Cx3cr1-deficient αSyn transgenic
169 mice at a minimally higher mean percent leukocyte area covered than for the Cx3cr1-competent group
170 (**Supplemental Figure 2A**). We observed, however, a significantly higher mean level of αSyn
171 accumulated in the submucosal plexus in αSyn transgenic mice lacking Cx3cr1 compared to αSyn
172 transgenic mice expressing Cx3cr1 ($p = 0.001$, two-way ANOVA with Tukey HSD post-hoc analysis;
173 **Figure 4A**). Consistent with the Cx3cr1-sufficient αSyn transgenic mice, no overt increased
174 accumulation of αSyn was observed in the myenteric plexus **(Figure 4B)**. These results indicate a
175 potential link between monocyte/macrophage signaling and αSyn accumulation in ENS in this
176 experimental IBD model.
177
178 ***Systemic IL-10 ameliorates DSS-induced colitis and associated enteric αSyn accumulation in αSyn***
179 ***transgenic mice***
180 Interestingly, we observed above that LPS-induced colonic leukocyte infiltration did not result in
181 increased accumulation of αSyn in the ENS of the colon and that the main difference in cytokine
182 expression between the DSS and LPS paradigms was increased IL-10 expression in the LPS group
183 (**Figure 4**). Interleukin-10 is an important regulator of monocytes/macrophages, and genetic ablation
184 of IL-10 signaling or blocking IL-10 with specific antibodies was shown to enhance DSS colitis (44,

45). To mimic the effect of higher levels of IL-10 in an acute model of DSS colitis, we administered intravenously murine IL-10 (mIL10), which was recombinantly engineered onto two different murine IgG variants to extend the half-life of mIL-10 in circulation (mIgG1(v1)-mIL10 and mIgG1(v2)-mIL10, respectively). As shown previously, DSS induced a marked increase in leukocyte infiltration and αSyn accumulation, which was similar in the untreated and control IgG treated group (**Figure 6A, B**). Both mIgG1(v1)-mIL10 and mIgG1(v2)-mIL10 significantly reduced leukocyte infiltration despite administration of DSS ($p<0.0001$, one-way ANOVA with Tukey HSD post-hoc analysis; **Figure 6A, B**). Also, both mIgG1-mIL10 variants had reduced mean levels of human αSyn in the submucosal plexus whereas mIgG1(v2)-mIL10 reached significance ($p=0.02$, one-way ANOVA with Tukey HSD post-hoc analysis; **Figure 6B**). Interestingly, the significantly reduced αSyn accumulation was associated with detectable serum exposure of mIgG1(v2)-mIL10 whereas mIgG1(v1)-mIL10 was no longer detectable at the end of the in vivo phase, after 7d (**Figure 6C**). These results underline further an important role for the IL-10 pathway in keeping αSyn accumulation at a reduced level throughout the course of experimental IBD. Together, the genetic and pharmacological modulation of DSS colitis corroborates a relevant role for monocyte/macrophage pathways in the development of αSyn accumulations in the ENS of the colon.

Experimental colitis-induced enteric αSyn accumulation at young age persists for months and exacerbates brain pathology and dopaminergic cell loss in old αSyn transgenic mice

The previously highlighted hypothesis by Braak and colleagues associates αSyn brain pathology with previous development of αSyn pathology in the ENS (5, 46). However, it is currently unknown whether previous inflammatory conditions propel this ENS αSyn accumulation that may further worsen αSyn aggregation in the brain. To test this, we first explored αSyn accumulation in the submucosal plexus of (Thy1)-h[A30P]αSyn transgenic mice that had experienced DSS colitis previously but had fully recovered two months later. As expected, leukocyte infiltration in the submucosal plexus had returned to normal levels following the two-month recovery period (**Supplemental Figure 3A**). Remarkably however, αSyn accumulation in the ganglia of the submucosal plexus was still almost two-fold higher when compared to αSyn transgenic mice that were

not exposed to DSS, and this was exacerbated in αSyn transgenic mice deficient for Cx3cr1 (**Supplemental Figure 3B**).

To assess development of brain αSyn pathology, we exposed 3-month old hemizygous (Thy1)-h[A30P]αSyn transgenic mice to DSS or normal drinking water (chronic increasing dose paradigm) and then returned all to normal drinking water (**Figure 2C**). After aging up to 9 or 21 months of age (i.e. mice aged for an additional 6 or 18 months after the chronic DSS paradigm), various brain regions were analyzed for pathologically accumulated αSyn (proteinase K resistant, pSer129-αSyn immunoreactive inclusions). Twenty-one-month old mice that only received water during their lifetime showed low levels of pathological αSyn inclusions in the brain (**Figure 7 and Supplemental Figure 4**), which is consistent with previous observations in the brain of the hemizygous (Thy1)-h[A30P]αSyn transgenic mice (47). In marked contrast, the majority of 21-month-old and previously DSS-exposed hemizygous (Thy1)-h[A30P]αSyn transgenic mice presented with higher degrees of pathological αSyn in the same brain areas where mice on water displayed much lower pSer129-positive immunoreactivity, reminiscent of the homozygous (Thy1)-h[A30P]αSyn transgenic mice (47). Intriguingly, αSyn transgenic mice that were aged to 9 months presented with extremely low levels of pathological αSyn inclusions in the brain (**Figure 7 and Supplemental Figure 4**). For the αSyn transgenic mice that aged up to 21 months, the accumulated αSyn pathology recorded in the SN was accompanied by a significant loss of tyrosine hydroxylase (TH) and Nissl positive cells ($p \leq 0.05$, Student's T-test; **Figure 8**). Together, DSS colitis at a young age caused an age-dependent exacerbation of αSyn inclusion pathology and a loss of nigral dopaminergic cells in the brain of αSyn transgenic mice, similar to the human neuropathological hallmarks of PD.

Discussion

Currently, there is no therapy for PD available to slow or stop its progression and an obstacle in the quest to develop one is that we do not understand the triggers of PD (48). Intraneuronal accumulation of aggregated αSyn (i.e. Lewy bodies and neurites) is a key neuropathological hallmark, thus the distribution of Lewy pathology in postmortem brain tissues has been used for disease staging in PD (2, 4, 46). Abnormal accumulation of αSyn has also been observed in the peripheral nervous system in PD and in some individuals at risk of developing the disease (49, 50). Similar to this finding in people, αSyn immunoreactive inclusions have also been detected in the ENS of a transgenic mouse model prior to changes in the CNS (51). It is also suggested, based on preclinical models and postmortem pathology in various organs including the brain, that αSyn pathology propagates in a temporospatial and prion-like manner (2, 4, 5, 52, 53). However, the initial factors triggering αSyn aggregation are yet to be established (48). Moreover, the involvement of peripheral stimuli in the aggregation and pathogenic spread of αSyn is only beginning to unravel.

In this study, we provide evidence that patients with IBD have increased αSyn accumulation in their ENS (**Figure 1**) and that an experimental IBD-like inflammation (DSS colitis) triggers αSyn accumulation in the ENS of wildtype mice and in a transgenic mouse model of PD (**Figure 3**). Interestingly, in IBD patients and in the mouse model of IBD, macrophages filled with αSyn could be observed in the inflamed area (**Figure 5**). Aggravation of enteric αSyn accumulation in αSyn transgenic mice lacking Cx3cr1 signaling and amelioration of inflammation and enteric αSyn load by systemic IL-10 suggest a modulatory role of monocytes/macrophages in this process (**Figure 4 and 6**). Remarkably, we further observed that the aggravation of αSyn accumulation in the ENS persisted even after two months of recovery from DSS colitis, indicating that the observed effect is not a transient phenomenon (**Supplemental Figure 3**). Most importantly, 18 months but not 6 months post DSS colitis, αSyn transgenic mice had developed Parkinson-like brain pathology (**Figures 7 and 8 and Supplemental Figure 4**). This included elevated proteinase K resistant pSer129-αSyn pathology in the midbrain, including the SN, and other brain regions and an average decrease of 30-50% of TH- and Nissl positive cells in the SN. Together, this colitis model recapitulated the proposed

accumulation of αSyn in the ENS in wildtype and αSyn transgenic mice long before clinical diagnosis of PD in humans. Additionally, the subsequent age-related development of αSyn pathology together with the loss of nigral dopaminergic neurons in the brain of αSyn transgenic mice mimicked a progression of the disease similar to what is proposed in humans.

We established that a mechanism by which peripheral inflammation promote αSyn accumulation in the colon potentially involves monocytes and macrophages. Interestingly, both peroral DSS and peritoneal LPS administration provoked strong local immune reactions resulting in leukocyte infiltration into the submucosa of the colon. This inflamed region is anatomically right next to the submucosal plexus and is separated by a muscular layer from the myenteric plexus (**Figure 2**). This might explain why the effect of αSyn accumulation was only observed in the nerves of the submucosal plexus but not in the ganglia of the myenteric plexus in our (Thy1)-h[A30P]αSyn transgenic mouse model of colitis. The mechanism underlying how intraperitoneally administered LPS leads to submucosal leukocyte infiltration probably involves the monocyte attractant chemokine CCL2 (**Figure 4**), but the specifics remain unclear. CCL2 was also upregulated in the colon of our DSS model. However, in contrast to peritoneal LPS, where infiltration of macrophages followed a patchy pattern, DSS-related macrophage infiltration was distributed across the whole submucosa. Also, the primary mechanism of peroral administered DSS is to destruct the mucosa of the colon, similar to some forms of ulcerative colitis, resulting in the transient disintegration of the intestinal epithelial barrier. The subsequent immune response to the infiltration of commensal bacteria evoked also in our (Thy1)-h[A30P]αSyn transgenic mouse model the expression of cytokines such as IL-1β and IL-6. This upregulation was absent in the LPS paradigm that had an intact mucosa. By acting on tight junctions, IL-1β and IL-6 can increase intestinal barrier permeability (gut leakiness), facilitating the recruitment of additional immune cells to the site of the inflammatory signal eventually culminating in widespread immune activation (54, 55). Consistent with the breach of barrier permeability in our mouse model, some PD patients express increased colonic cytokines such as IL-1β, IL-6 and TNF, occurring together with increased intestinal permeability (29, 56). In this context, it is striking that IBD patients on anti-TNF therapy have a reduced risk of developing PD (37). Here we

289 demonstrate that patients with IBD also present with αSyn accumulations in the ENS as well as in
290 infiltrating leukocytes nearby. In this regard, it is interesting to note that mucosal macrophages with
291 intralysosomal αSyn content were previously described in the intact human appendix (57). These
292 macrophages were in close proximity to the axonal varicosities of the vermiform appendix which
293 showed an enriched staining for αSyn in the mucosal plexus. Indeed, we recently demonstrated that
294 the vermiform appendix contains aggregated and truncated αSyn that has the propensity to aggregate
295 recombinant αSyn *in vitro* (18). Also, monomeric and oligomeric αSyn species reportedly act as
296 chemoattractants for neutrophils and monocytes, enhancing the maturation of dendritic cells in the
297 ENS (28, 58). With such a role in intestinal immunity therefore, it is possible that the strong tissue
298 destruction induced by DSS in the present study released αSyn, which perhaps served as a
299 chemoattractant for monocytes. It is likely that increased abundance of extracellular αSyn and altered
300 intestinal permeability, along with the DSS-evoked inflammatory response may have provided an
301 enabling milieu allowing further αSyn accumulation in the ENS of the colon (59). However, the
302 pathways leading to αSyn accumulation in macrophages remain to be elucidated. Mechanistically, it
303 has been shown that excess endogenous αSyn compromises phagocytic activity in human iPSC-
304 derived macrophages (60). Macrophages and other immune cells are also regulated by LRRK2, an
305 established risk gene for PD and IBD. It will be interesting to explore in our colitis paradigm the
306 effect of LRRK2 (e.g. its effect on autophagy in macrophages (34, 35, 61)) and other pathways in
307 macrophages on αSyn accumulation.

308 Most profoundly, besides the accumulation of αSyn in the submucosal plexus, we found that a single
309 chronic DSS paradigm at young age exacerbated αSyn pathology in the CNS of (Thy1)-h[A30P]αSyn
310 transgenic mice much later in life (**Figure 7**). But how does this severe αSyn inclusion pathology
311 develop in the brain of these mice? One hypothesis is that the brain αSyn pathology observed in this
312 study could be due to direct effects of peripheral immune activation on the brain and brain
313 vasculature. Hypothetically, colitis induced by DSS or LPS could compromise both active and passive
314 components of the blood-brain barrier, which may render the CNS vulnerable to immune cells from
315 the periphery (62, 63). Alternatively, certain peripheral triggers can directly affect microglial activity

316 in the brain. For instance, short-chain fatty acids derived from gut microbiota appear to regulate
317 function and maturation of microglia in the mouse CNS (64) and inflammatory mediators from gut
318 microbiota could be carried in the bloodstream and induce pathological and behavioral changes in an
319 αSyn transgenic mouse model (65). Moreover, rats and nematodes develop αSyn inclusions after
320 exposure to the bacterial amyloid protein curli, a protein which stimulates microgliosis, astrogliosis,
321 and secretion of IL-6 and TNF (66). Intriguingly, a recent study reported that peripherally applied
322 inflammatory stimuli induce acute immune training (that exacerbates β-amyloid pathology) and
323 immune tolerance in the brain that reprograms microglia, an effect which can persist for at least six
324 months (67).

325 Another hypothesis is that the brain αSyn pathology observed may have accumulated following the
326 transfer of pathogenic αSyn seeds from the gut via the vagal nerve. It is already established in rodents
327 and non-human primates that αSyn pathology in the CNS can propagate from cell to cell, perhaps in a
328 prion-like fashion (52, 53, 68, 69) and that certain pathogenic forms of αSyn may serve as templates
329 in recipient cells, seeding and inducing further aggregation of endogenous αSyn in these cells (68, 70–
330 72). Interestingly, several studies in preclinical *in vivo* models have demonstrated that pathogenic
331 αSyn seeds can be transferred from the peripheral nervous system to the CNS. Indeed, aggregated
332 recombinant αSyn injected intraperitoneally, intramuscularly or into the gastric wall of certain mouse
333 models of PD results in αSyn inclusions in the CNS (24, 73), with the latter being transmitted via the
334 vagal nerve (74). Another study showed that vagotomy in mice prevents propagation of pathology
335 into the CNS (74), a finding that is parallel to a peripheral rotenone-related αSyn rat model in which
336 vagotomy reduced propagation of αSyn pathology (75), and to a human study that reported that
337 vagotomy in a Danish population also decreases the risk of PD (27). Similarly, after injection of PD
338 brain lysate and recombinant αSyn into the intestinal wall αSyn pathology trafficked through the
339 vagal nerve to the dorsal motor nucleus of the vagus (23). Others have shown that virus-based
340 expression of human αSyn in the medulla oblongata resulted in a transfer of αSyn towards rostral
341 brain regions in a rat model (76). The findings in these previous studies, along with the present
342 findings recall the Braak hypothesis and highlight the critical connection of the vagal nerve. Indeed, in

the present study, αSyn pathology was much more prominent in the reticular nucleus (including the vagal area) and midbrain areas (compared to the rostral areas) 18 months post DSS colitis, suggesting the potential involvement of this nerve in the accumulation of αSyn in the CNS.

In summary, here we report that individuals with IBD exhibit αSyn accumulation in the colon concomitant with infiltrating monocytes/macrophages positive for αSyn. Employing a experimental model of IBD, we provide proof-of-principle demonstrating that αSyn accumulated in the colon of (Thy1)-h[A30P]αSyn transgenic and wildtype mice upon DSS colitis and that this process can be modulated by monocyte/macrophage-related signaling. We further demonstrate that chronic DSS colitis in young (Thy1)-h[A30P]αSyn transgenic mice robustly exacerbated αSyn accumulation in the aged brain which was accompanied by reduced numbers of TH- and Nissl positive neurons in the nigra. The present findings are in consonance with retrospective and cohort studies demonstrating a link between IBD and PD in various populations including those in Taiwan, Denmark and the US (36, 37, 77), although this may not be the case in all populations (78). The exact mechanisms connecting the gut pathology to the pathology in the brain including the role of monocytes/macrophages, remain to be established. In conclusion, this novel mouse model of a potential preclinical stage of PD recapitulated the accumulation of αSyn in the ENS and the subsequent age-related development of brain pathology. Together, our data suggest a critical role for intestinal inflammation in the initiation and progression of PD.

Methods

Mice

Male C57BL/6 wild type mice (Jackson Laboratories, Bar Harbor, USA), hemizygous Tg(Thy1-SNCA*A30P)18Pjk ((Thy1)-h[A30P]αSyn) (39) and Tg(Thy1-SNCA*A30P)18Pjk crossed with Cx3cr1tm1Litt ((Thy1)-h[A30P]αSyn /CX3CR1-def; homozygous for Cx3cr1-GFP knock-in allele; (79) transgenic mice were used for the study. (Thy1)-h[A30P]αSyn transgenic mice express mutant human αSyn under the neuron selective Thy1 promoter. (Thy1)-h[A30P]αSyn transgenic mice were crossed to Cx3cr1-def transgenic mice which express eGFP replacing fractalkine gene expression. All mice were maintained on a C57BL/6 background for more than 10 generations and under specific pathogen-free conditions. To the extent possible, littermates were used in the experiments. Health status was monitored daily during experiments.

Human Subjects

Samples from patients with Crohn's disease (CD), ulcerative colitis (UC) or healthy subjects (HS) were provided by the tissue bank, Institute of Pathology, University of Bern. Briefly, specimens were obtained from patients who underwent surgical procedures at the University Hospital (Inselspital) in Bern, Switzerland between 2004 and 2011. Three selected male patients previously clinically diagnosed with UC with a reported disease duration > 6 year (n=3) and undergoing steroid therapy combined with either metronidazole or mesalazine. CD patients were of mixed gender and aged 22-56 years ranging from 2 months to 11 years post disease diagnosis undergoing treatment with either infliximab or mesalazine in combination with steroids. Healthy subjects were of mixed gender with no report of inflammatory bowel disease, aged 40-59. All samples contained the mucosa and submucosa regions including minor parts of the circular muscle layer. Following surgical removal, tissue samples were immediately immersed in O.C.T. compound (VWR International GmbH, Dietikon, Switzerland), frozen in liquid nitrogen and stored at -80°C. Diagnosis of disease status was made according to established criteria for histopathological analysis.

388 ***Experimental IBD in mice with DSS and LPS***

389 Paradigms for the induction of inflammation were either 1 week (acute) or 3-4 weeks (chronic) with
390 or without an incubation phase of 2, 6 or 18 months post application (**Figure 2**). Acute systemic
391 inflammation was induced by intraperitoneal Lipopolysaccharide (LPS) application (80) of 0.5 mg/kg
392 in 100 µl injection volume on day 1 and 4 (Sigma-Aldrich Chemie GmbH, Steinheim, Germany, LPS
393 055:B5). Acute colitis was induced by application of 36-50kDa Dextran Sulfate Sodium (DSS) (81)
394 (160110, MP Biomedicals, LLC, Illkirch, France) at 0%, 1%, 2.5% or 5% in autoclaved drinking
395 water for 5 continuous days respectively, followed by 2 days of water (1 DSS application cycle).
396 Chronic colitis was achieved by 4 repeating DSS application cycles. The DSS concentration during 4
397 weeks of chronic colitis was either 1% or 2.5% for 4 weeks or 2.5%-4% raised 0.5% every week for 4
398 weeks. Mice from same littermate group were randomized per cage into vehicle and inflammation
399 inducing agent.
400
401 ***IL-10 treatment and exposure measurement***
402 Two different forms of mouse IgG bound murine IL-10 (mIgG(v1)-mIL10 and mIgG(v2)-mIL10)
403 were diluted in pre-prepared sterile formulation buffer comprised of 0.5% mouse serum supplemented
404 with 25mM citrate, 300mM arginine to a final concentration of 0.75mg/ml and the pH adjusted to 6.7
405 on the day of application. Each mouse was treated once with 150 µg i.p concurrently with the
406 initiation of the acute colitis paradigm with 5% DSS. The concentrations of mIgG-mIL10 fusion
407 proteins in murine serum samples were determined by enzyme-linked immunosorbent assays (ELISA)
408 specific for the Fab moiety of the administered mIgG-mIL10 fusion protein. Biotinylated mIgG-
409 mIL10-specific target molecules were used for capturing, goat anti-mIg IgG-HRP conjugate and
410 peroxidase substrate ABTS was used for quantitative detection of mIgG-mIL10 fusion proteins.
411
412 ***Immunohistochemistry***
413 Animals were injected with a lethal dose of pentobarbital (150 mg/kg). Upon full anesthesia, mice
414 received transcardial perfusion with room temperature phosphate buffered saline (PBS). For
415 biochemical and immunohistochemical analysis, one section of either the proximal colon was fresh

frozen and stored at -80°C or post-fixed in 4% paraformaldehyde (PFA) solution for 24 h. Following post-fixation, organs were incubated in 30% sucrose/PBS at 4°C for at least 48 h before further processing. Subsequently, enteric tissue was cryotome-sectioned to 35 µm thick longitudinal sections (approx. 1 cm length). The brain was collected and post-fixed for 24 h in 4% PFA followed by 30% sucrose in phosphate buffer until cryo-sectioning of floating sections at 40 µm. Histological analysis of the colon was performed using standard hematoxylin staining. Immunohistochemical staining was accomplished using the Vectastain Elite ABC Kits and Peroxidase Substrate Kit SK-4100 (Vector Laboratories, Burlingame, CA, USA) or fluorescently labelled secondary antibodies (Alexa coupled to dye 488, 555 or 647, Life Technologies, Zug, Switzerland). The following primary antibodies have been used for overnight incubation at a dilution of 1:1000: monoclonal antibody to human α-synuclein (sc-12767, Santa Cruz Biotechnology, Heidelberg, Germany), polyclonal antibody to murine α-synuclein (Syn1, BD Transduction Laboratories, Allschwil, Switzerland), polyclonal antibody to the peripheral neuronal marker Peripherin (Millipore Corporation, Billerica, MA, USA), and polyclonal antibody to macrophage marker Iba1 (Wako Chemical GmbH, Neuss, Germany). To detect phosphorylated αSyn (pSer129 pathology) in the free-floating brain sections, monoclonal antibody (ab51253, Abcam, Cambridge, USA) to human αSyn was used at a dilution of 1:10000. Prior to the pSer129 staining, the free-floating brain sections were incubated for 10 min at room temperature in a phosphate buffered saline solution containing 10 µg/mL proteinase K (Cat # 25530015; Invitrogen, California, USA). TH-immunoreactive cells were detected using a polyclonal antibody (657012, Millipore Sigma) at a dilution of 1:1000. To measure the density of Nissl-positive cells, the TH-stained cells were counter-stained with Cresyl violet. The slides were incubated in 0.1% Cresyl violet solution for 9 min and then dehydrated in 95% and 100% ethanol and then xylene prior to coverslipping with Cytoseal 60 mounting media (Thermo Fisher Scientific). Quantifications of the blind-coded TH/Nissl stained slides were done using Stereoinvestigator (version 2017.01.1; MBF Bioscience, Williams, VT, USA) on Imager M2 microscope (ZEISS) coupled to a computer. We analyzed 5-7 nigral sections per animal, and a total of 7-8 animals per treatment group. We outlined the substantia nigra pars compacta and counted every TH-immunoreactive and Nissl-positive cell in that area and computed the number of cells per section, generating the mean cell density per animal.

444 We then calculated the mean density of cells per treatment group and analyzed the data using
445 unpaired Student's T-test after confirming normality and homoscedasticity in Prism 7.0 (GraphPad
446 Software).
447
448 ***Imaging and stereological quantification of αSyn deposits in enteric nervous system***
449 Imaging and stereological quantification was performed on a Zeiss Axio Imager Z2 fluorescence
450 microscope (Carl Zeiss AG, Jena, Germany). Leica TCS SP5 confocal system using an HCX PL APO
451 CS 40x 1.3 oil UV or an HCX PL APO LB 63x 1.4 oil UV objective was utilized for image recording.
452 Accumulation of αSyn in the ENS was assessed on a random set of 3 adjacent 35 µm thick, αSyn-
453 immunostained sections comprising the myenteric and submucosal neuronal plexuses. Analysis was
454 performed with the aid of Stereologer software (Stereo Investigator 10, MBF Bioscience, Williams,
455 VT, USA) as described previously (82). In the myenteric plexus ganglion volume was defined by
456 multiple outlined plexuses containing a range of 5-20 neuronal cells and quantified by the optical
457 fraction fractionator technique. In contrast to the myenteric plexus, the submucosa consists of
458 compact plexuses with 1-5 cells including interconnecting neurites. Therefore, the entire submucosa
459 was set as region of interest, analyzed with the area fraction fractionator technique. Results of the
460 submucosal plexus are displayed by percent area containing αSyn deposits. For the IL-10 experiment,
461 αSyn positive granules from immunofluorescence images were counted for each image. Granules
462 were filtered based on having a size between 12 and 50000 pixels and a minimal intensity value
463 greater than 300. The filtering step was included to exclude small background particles and
464 macrophages (very large spots). The counts were then aggregated to the animal level by summing the
465 granule counts of all images per animal and then normalizing for (i.e. dividing by) the number of
466 images for a given animal. Upon exploratory data analysis two animals were excluded: one mouse
467 because it only had one image and another due it being an outlier, based on its infiltration score and
468 image data.
469
470
471

Blinding

For analyses of colon and brain tissue on slides, a second individual assigned unique codes to stained slides. Therefore, the experimenter conducted the analyses blinded to the identity of the mice. For randomization of treatment groups see above.

Quantification of leukocytes infiltration

To determine the leukocyte covered area in the colon after LPS or DSS application, three adjacent hematoxylin stained sections were quantified. Total area of colon sections and localizations of leukocyte assemblies within the tissue architecture were identified and outlined utilizing Stereologer Software (Stereo Investigator 6, MBF Bioscience, Williams, VT, USA). Percentage of leukocyte covered area has been set in proportion to total area of the analyzed colon section. For the IL-10 experiment, hematoxilin stained colon slices were examined by an expert pathologist blinded to treatment conditions. A score of 0-3 was assigned to each section for each of the 3 layers lamina propria, submucosa and muscularis based on the degree of inflammatory infiltration. A score of 0 denoted no inflammation and a score of 3 indicated extensive infiltration. The mean of the values for all 3 layers was taken as the final measure of leukocyte infiltration per mouse.

Quantification of αSyn/Iba1 double positive macrophages

The number of α-syn+/Iba1+ positive cells was evaluated by quantification of 10 random regions in 2 adjacent sections of the proximal colon. The region of interest was set to contain the myenteric plexus/circular muscle layer and the submucosal plexus. Cells were assessed for positive αSyn staining and concomitant co-localization with the macrophage marker Iba1 was quantified.

Scoring of pSer129 pathology and brain heatmap

We evaluated pSer129 pathology on a full series of immunostained coronal sections from 10 mice per treatment group (i.e. water vs. DSS-treated groups) on blind-coded slides using a previously described method (83). We visualized pathology from one hemisphere of all brain sections (apart from the

olfactory area) using NIKON Eclipse Ni-U microscope and assigned scores ranging from 0 to 4 to each brain area based on the relative abundance of PK-resistant pSer129-positive inclusions (i.e. cell bodies and neurites). In this case, 0 = no aggregates, 1 = sparse, 2 = mild, 3= dense, 4 = very dense. For the heatmap, we obtained the average score values of each brain area for each treatment group. The average data for each treatment group (n=10/ group) was then represented as a heatmap in a sagittal mouse brain background (http://atlas.brain-map.org/atlas?atlas=2#atlas=2&structure=771&resolution=16.75&x=7755.7470703125&y=3899.625&zoom=-3&plate=100883867&z=5).

Densitometry of pSer129 αSyn brain pathology

The density of pSer129 pathology in 12 major brain areas (reticular nucleus, pontine reticular nucleus, periaqueductal gray, gray and white layer, reticular formation, substantia nigra, ventral tegmental area, thalamus, hypothalamus, central amygdala, pallidum and striatum) was determined in the water and DSS-treated animals. A NIKON Eclipse Ni-U microscope was used to acquire 20x magnification images (without condenser lens) from all the indicated brain areas, using the same exposure time for all images. In all cases, images were acquired on three sections separated by 420 µm intervals (localized between Bregma). We then processed the acquired images using Image J64 (84), created a mask (to exclude background) that redirects to the original image for analysis, measured the total area and the mean grey value of the area that had inclusions. For brain areas such as periaqueductal gray that do not fill the entirety of the field to be analyzed, we drew a contour of the area and the analysis was performed only within that contoured area. We subsequently calculated the grey value of the area per square pixels for each image (i.e. A.U./px^2 = mean grey value x area stained/total area assessed). Based on this, we calculated the average grey value per square pixels for each brain area for each animal (n = 6 mice/group), and then extended this calculation to determine the average grey value per square pixels for each treatment group and each of the twelve brain areas of interest.

527 ***mRNA expression***

528 To assess mRNA expression levels from the proximal colon, RNA was extracted from fresh frozen
529 tissue with MagnaLyser green beads (Roche Diagnostics, Mannheim, Germany) and Qiazol Lysis
530 (Reagent cat.no.79306, Hilden, Germany) purified on MagnaPure LC (HP Kit no.03542394001, F.
531 Hoffmann - La Roche AG, Rotkreuz, Switzerland) and amplified via real-time PCR (4ng
532 RNA/reaction; Lightcycler 480, Roche Diagnostics Corporation, Indianapolis, USA). Amplification
533 of mRNA was performed by using TaqMan probes for human or murine specific α-synuclein and for
534 selected cytokines/chemokines (Applied Biosystems Europe B.V., Zug, Switzerland). Target mRNA
535 was normalized to tissue-specific murine GAPDH levels and displayed as relative expression after 30
536 amplification cycles.
537
538 ***Statistics***
539 Statistical analysis of gut pathology and inflammation was performed using GraphPad Prism 6.04 or
540 7.0 software (GraphPad Software, Inc. La Jolla, CA, USA). The results are expressed as mean values
541 ± standard errors of the mean (SEM). Student's T-test (or Welch's T-test for unequal variances) was
542 used to compare two groups and ANOVA was used for multi-comparison of groups followed by
543 Tukey HSD post-hoc analysis. For the statistical analysis of the pSer129 αSyn brain pathology,
544 negative-binomial mixed-effects models with a random intercept for each sample were used to
545 analyze the dataset via the 'lme4' (http://lme4.r-forge.r-project.org/) package in R v 3.4.4. To analyze
546 the pSer129 αSyn cell count dataset, an offset for the total area examined was included to model the
547 densities. Linear contrasts with false discovery rate (FDR) adjustments were then used to test our
548 hypotheses and account for multiple testing (for brain area and experimental group). Like the pSer129
549 dataset, the Iba-1/αSyn-double positive dataset were analyzed using negative-binomial regression and
550 Tukey HSD adjusted contrasts to test our hypotheses.
551
552 For the mRNA expression analysis, data quality was assessed by inspecting the distribution of Cp
553 values of reference endogenous genes across samples, by inspecting the level of Cp variation between
554 technical replicates and by exploring the samples multivariate signal distribution as in a principal

555 component analysis. Relative gene expression levels were expressed as $2^{-(Cpgene - CpRef)}$. Statistical
556 analyses to assess the effect of the experimental conditions on the log2 gene expression levels were
557 done with linear models using the *limma* package (Bioconductor/R, Smyth, 2005). These analyses
558 were implemented in R v3.1.1.
559
560 For the statistical modelling of the effects of the IL-10 treatment on αSyn counts, as well as
561 infiltration scores, the levels for IgG1(v1)-IL10 and IgG1(v2)-IL10 treatment were compared to the
562 positive (vehicle/DSS) control. Additionally, since levels of the control antibody treatment (IgG1(v1))
563 were very similar to the positive control, the two groups were pooled in further contrasts in which
564 effects of individual antibodies or control IgG was assessed. For αSyn counts, a linear model on the
565 treatment groups with one-degree freedom contrasts was applied. For the infiltration score a Kruskal-
566 Wallis test, with the same contrasts, was used.
567
568 ***Study approval***
569 The human subjects' study was conducted with the approval of the local Ethical Committee in Bern
570 No. 47/04. Written informed consent was obtained from each patient. The animal experiments were
571 approved by a Roche internal review board and the local authorities.

572 **Author contributions**

573 S.G., N.M. and L.S. planned and performed the in vivo experiments, colon immunostaining, analysis,
574 and quantification; S.G. and N.M. drafted a first version of the manuscript; E.Q. performed, imaged,
575 quantitated pSer129, TH and Nissl staining in the brain sections, and drafted a more advanced version
576 of the manuscript with J.A.S., who also provided helpful discussion. F.B. and K.O.S. supported the
577 image acquisition and image analysis for the colon samples; M.St. performed imaging and data
578 analysis of experiments with wildtype mice; G.D.P. and J.S.P. performed statistical analysis of the
579 DSS experiments; H.R. and M.H. performed mRNA analyses; M.Se. trained S.G. and L.S. on mouse
580 necropsy and supported their work; P.M. performed expert pathology staging on leukocyte
581 infiltration; T.E. and A.W. provided mIgG-mIL-10 fusion proteins and measured serum exposure;
582 Z.M. performed statistical analysis for the pSer129 αSyn immunohistochemistry data. M.L.E.G.
583 provided helpful discussion and project planning. A.H. co-mentored S.G. and N.M., performed expert
584 pathology staging on leukocyte infiltration and contributed to experimental planning. C.M. trained
585 S.G. on the colitis model, provided human tissue and expert input on the experimental IBD model.
586 M.B. and P.B. co-mentored Roche Postdoctoral Fellows S.G. and N.M., conceived and oversaw the
587 study, and performed experimental planning; M.B., P.B. and E.Q. wrote the final version of the
588 manuscript.
589

590 **Acknowledgments**

591 We acknowledge the human donors for providing tissue used in this study. We thank Drs. L. Ozmen,
592 A. Bergadano, and A. Su for their tremendous support in maintaining the mouse colony and
593 establishing of relevant animal experiment licenses, and we are grateful to the animal care takers,
594 veterinarians and many unnamed staff at Roche for their valuable work with the mice in this study. In
595 addition, at Roche we thank Dr. K.G. Lassen for critical input to the paper, Dr. C. Ullmer for co-
596 mentoring S.G. and providing scientific input, Dr. L. Collin for helping with confocal imaging and we
597 are grateful to Dr. T. Kremer, N. Haenggi, D. Mona, A. Girardeau, and J. Messer for providing
598 support in tissue dissections and G. Walker and R. Lauria for technical support. Ms. E. Schulz from
599 VARI assisted with immunostaining of the brain tissue. We thank the Contract Research Organization

Frimorfo for carefully sectioning the brains for this study. We acknowledge Drs. L. Gaudimier (née Chicha) and F. Pan-Montojo for scientific discussions early in the project and Dr. W. Zago from Prothena for valuable scientific input throughout the project. P.B. reports relevant grants from NIH (R01DC016519-01, 1R21NS106078-01A1 and 5R21NS093993-02), Department of Defense (W81XWH-17-1-0534), The Michael J. Fox Foundation for Parkinson's Research, and Cure Parkinson's Trust. Finally, we thank the Roche Postdoctoral Fellowship Program for supporting S.G. and N.M.

Conflicts of Interest

At the time of the study S.G. and N.M. were Roche Postdoctoral Fellows employed by Roche and L.S., F.B., G.D.P., J.S.P., K.O.S., H.R., M.H., M.Se. M.St., P.M., A.W., T.E., A.H. and M.B. are or were fulltime employees or trainees at Roche and they may additionally hold Roche stock/stock options. S.G. and L.S. are currently employees of Neurimmune AG, Schlieren, Switzerland. P.B. has received commercial support as a consultant from Renovo Neural, Roche, Teva, Lundbeck A/S, AbbVie, NeuroDerm, Fujifilm Cellular Dynamics, Living Cell Technologies, IOS Press Partners, and Axial Biotherapeutics. Additionally, P.B. has received commercial support as a consultant from Renovo Neural, Roche, Teva, Lundbeck A/S, AbbVie, NeuroDerm, Fujifilm Cellular Dynamics, Living Cell Technologies, IOS Press Partners, Axial Biotherapeutics and CuraSen. Additionally, P.B. has received commercial support for grants/research from Renovo, Roche, Teva, and Lundbeck. P.B. has ownership interests in AcouSort AB. The other authors do not have conflicts of interest with regard to this research.

621 **References**

622 1. Tysnes O-B, Storstein A. Epidemiology of Parkinson's disease. *J Neural Transm (Vienna)*
623 2017;124(8):901–905.

624 2. Spillantini MG et al. Alpha-synuclein in Lewy bodies. *Nature* 1997;388(6645):839–840.

625 3. Spillantini MG, Goedert M. Neurodegeneration and the ordered assembly of α-synuclein. *Cell*
626 *Tissue Res.* 2017;373(1):137–148.

627 4. Braak H et al. Staging of the intracerebral inclusion body pathology associated with idiopathic
628 Parkinson's disease (preclinical and clinical stages). *J. Neurol.* 2002;249 Suppl 3:III/1-5.

629 5. Del Tredici K, Braak H. Lewy pathology and neurodegeneration in premotor Parkinson's disease.
630 *Mov. Disord.* 2012;27(5):597–607.

631 6. Polymeropoulos MH et al. Mutation in the alpha-synuclein gene identified in families with
632 Parkinson's disease. *Science* 1997;276(5321):2045–2047.

633 7. Schrag A, Horsfall L, Walters K, Noyce A, Petersen I. Prediagnostic presentations of Parkinson's
634 disease in primary care: a case-control study. *Lancet Neurol* 2015;14(1):57–64.

635 8. Gaenslen A, Swid I, Liepelt-Scarfone I, Godau J, Berg D. The patients' perception of prodromal
636 symptoms before the initial diagnosis of Parkinson's disease. *Mov. Disord.* 2011;26(4):653–658.

637 9. Pont-Sunyer C et al. The onset of nonmotor symptoms in Parkinson's disease (the ONSET PD
638 study). *Mov. Disord.* 2015;30(2):229–237.

639 10. Berg D et al. The PRIPS study: screening battery for subjects at risk for Parkinson's disease. *Eur.*
640 *J. Neurol.* 2013;20(1):102–108.

641 11. Postuma RB, Gagnon J-F, Bertrand J-A, Génier Marchand D, Montplaisir JY. Parkinson risk in
642 idiopathic REM sleep behavior disorder: preparing for neuroprotective trials. *Neurology*
643 2015;84(11):1104–1113.

644 12. Abbott RD et al. Frequency of bowel movements and the future risk of Parkinson's disease.
645 *Neurology* 2001;57(3):456–462.

646 13. Savica R et al. Medical records documentation of constipation preceding Parkinson disease: A
647 case-control study. *Neurology* 2009;73(21):1752–1758.

648 14. Mahlknecht P, Seppi K, Poewe W. The Concept of Prodromal Parkinson's Disease. *J Parkinsons*
649 *Dis* 5(4):681–697.

650 15. Houser MC, Tansey MG. The gut-brain axis: is intestinal inflammation a silent driver of
651 Parkinson's disease pathogenesis?. *npj Parkinson's Disease* 2017;3(1):3.

652 16. Braak H, Del Tredici K. Neuroanatomy and pathology of sporadic Parkinson's disease. *Adv Anat*
653 *Embryol Cell Biol* 2009;201:1–119.

654 17. Braak H, de Vos RAI, Bohl J, Del Tredici K. Gastric alpha-synuclein immunoreactive inclusions
655 in Meissner's and Auerbach's plexuses in cases staged for Parkinson's disease-related brain
656 pathology. *Neurosci. Lett.* 2006;396(1):67–72.

657 18. Killinger BA et al. The vermiform appendix impacts the risk of developing Parkinson's disease.
658 *Sci Transl Med* 2018;10(465):eaar5280.

659 19. Lee JM et al. The Search for a Peripheral Biopsy Indicator of α-Synuclein Pathology for
660 Parkinson Disease. *J. Neuropathol. Exp. Neurol.* 2017;76(1):2–15.

661 20. Corbillé A-G et al. Evaluation of alpha-synuclein immunohistochemical methods for the detection
662 of Lewy-type synucleinopathy in gastrointestinal biopsies. *Acta Neuropathol Commun* 2016;4:35.

663 21. Donadio V et al. A new potential biomarker for dementia with Lewy bodies: Skin nerve α-
664 synuclein deposits. *Neurology* 2017;89(4):318–326.

665 22. Phillips RJ, Walter GC, Wilder SL, Baronowsky EA, Powley TL. Alpha-synuclein-
666 immunopositive myenteric neurons and vagal preganglionic terminals: autonomic pathway implicated
667 in Parkinson's disease?. *Neuroscience* 2008;153(3):733–750.

668 23. Holmqvist S et al. Direct evidence of Parkinson pathology spread from the gastrointestinal tract to
669 the brain in rats. *Acta Neuropathol* 2014;128(6):805–820.

670 24. Breid S et al. Neuroinvasion of α-Synuclein Prionoids after Intraperitoneal and Intraglossal
671 Inoculation. *J. Virol.* 2016;90(20):9182–9193.

672 25. Sargent D et al. "Prion-like" propagation of the synucleinopathy of M83 transgenic mice depends
673 on the mouse genotype and type of inoculum. *J. Neurochem.* 2017;143(1):126–135.

674 26. Manfredsson FP et al. Induction of alpha-synuclein pathology in the enteric nervous system of the
675 rat and non-human primate results in gastrointestinal dysmotility and transient CNS pathology.
676 *Neurobiol. Dis.* 2018;112:106–118.

677 27. Svensson E et al. Vagotomy and subsequent risk of Parkinson's disease. *Ann Neurol.*
678 2015;78(4):522–529.

679 28. Stolzenberg E et al. A Role for Neuronal Alpha-Synuclein in Gastrointestinal Immunity. *JIN*
680 2017;9(5):456–463.

681 29. Devos D et al. Colonic inflammation in Parkinson's disease. *Neurobiol. Dis.* 2013;50:42–48.

682 30. Mogi M et al. Interleukin-1 beta, interleukin-6, epidermal growth factor and transforming growth
683 factor-alpha are elevated in the brain from parkinsonian patients. *Neurosci. Lett.* 1994;180(2):147–
684 150.

685 31. Brás J, Guerreiro R, Hardy J. SnapShot: Genetics of Parkinson's disease. *Cell* 2015;160(3):570-
686 570.e1.

687 32. Witoelar A et al. Genome-wide Pleiotropy Between Parkinson Disease and Autoimmune
688 Diseases. *JAMA Neurol* 2017;74(7):780–792.

689 33. Umeno J et al. Meta-analysis of published studies identified eight additional common
690 susceptibility loci for Crohn's disease and ulcerative colitis. *Inflamm. Bowel Dis.* 2011;17(12):2407–
691 2415.

692 34. Gardet A et al. LRRK2 is involved in the IFN-gamma response and host response to pathogens. *J.*
693 *Immunol.* 2010;185(9):5577–5585.

694 35. Hakimi M et al. Parkinson's disease-linked LRRK2 is expressed in circulating and tissue immune
695 cells and upregulated following recognition of microbial structures. *J Neural Transm (Vienna)*
696 2011;118(5):795–808.

697 36. Lin J-C, Lin C-S, Hsu C-W, Lin C-L, Kao C-H. Association Between Parkinson's Disease and
698 Inflammatory Bowel Disease: a Nationwide Taiwanese Retrospective Cohort Study. *Inflamm. Bowel*
699 *Dis.* 2016;22(5):1049–1055.

700 37. Peter I et al. Anti-Tumor Necrosis Factor Therapy and Incidence of Parkinson Disease Among
701 Patients With Inflammatory Bowel Disease. *JAMA Neurol* 2018;75(8):939–946.

702 38. Wan Q-Y, Zhao R, Wu X-T. Older patients with IBD might have higher risk of Parkinson's
703 disease. *Gut* 2018;gutjnl-2018-317103.

704 39. Kahle PJ et al. Subcellular localization of wild-type and Parkinson's disease-associated mutant
705 alpha -synuclein in human and transgenic mouse brain. *J. Neurosci.* 2000;20(17):6365–6373.

706 40. Chassaing B, Aitken JD, Malleshappa M, Vijay-Kumar M. Dextran sulfate sodium (DSS)-induced
707 colitis in mice. *Curr Protoc Immunol* 2014;104:Unit 15.25.

708 41. Weber B, Saurer L, Schenk M, Dickgreber N, Mueller C. CX3CR1 defines functionally distinct
709 intestinal mononuclear phagocyte subsets which maintain their respective functions during
710 homeostatic and inflammatory conditions. *Eur. J. Immunol.* 2011;41(3):773–779.

711 42. Medina-Contreras O et al. CX3CR1 regulates intestinal macrophage homeostasis, bacterial
712 translocation, and colitogenic Th17 responses in mice. *J. Clin. Invest.* 2011;121(12):4787–4795.

713 43. Kostadinova FI et al. Crucial involvement of the CX3CR1-CX3CL1 axis in dextran sulfate
714 sodium-mediated acute colitis in mice. *J. Leukoc. Biol.* 2010;88(1):133–143.

715 44. Kang S et al. Intestinal epithelial cell-derived semaphorin 7A negatively regulates development of
716 colitis via αvβ1 integrin. *J. Immunol.* 2012;188(3):1108–1116.

717 45. Li B, Alli R, Vogel P, Geiger TL. IL-10 modulates DSS-induced colitis through a macrophage-
718 ROS-NO axis. *Mucosal Immunol* 2014;7(4):869–878.

719 46. Braak H et al. Staging of brain pathology related to sporadic Parkinson's disease. *Neurobiol.*
720 *Aging* 2003;24(2):197–211.

721 47. Neumann M et al. Misfolded proteinase K-resistant hyperphosphorylated alpha-synuclein in aged
722 transgenic mice with locomotor deterioration and in human alpha-synucleinopathies. *J. Clin. Invest.*
723 2002;110(10):1429–1439.

724 48. Johnson ME, Stecher B, Labrie V, Brundin L, Brundin P. Triggers, Facilitators, and Aggravators:
725 Redefining Parkinson's Disease Pathogenesis. *Trends Neurosci.* 2018;S0166-2236(18):30253–30254.

726 49. Shannon KM, Keshavarzian A, Dodiya HB, Jakate S, Kordower JH. Is alpha-synuclein in the
727 colon a biomarker for premotor Parkinson's disease? Evidence from 3 cases. *Mov. Disord.*
728 2012;27(6):716–719.

729 50. Lebouvier T et al. Colonic biopsies to assess the neuropathology of Parkinson's disease and its
730 relationship with symptoms. *PLoS ONE* 2010;5(9):e12728.

731 51. Kuo Y-M et al. Extensive enteric nervous system abnormalities in mice transgenic for artificial
732 chromosomes containing Parkinson disease-associated α-synuclein gene mutations precede central
733 nervous system changes. *Hum Mol Genet* 2010;19(9):1633–1650.

734 52. Luk KC et al. Pathological α-synuclein transmission initiates Parkinson-like neurodegeneration in
735 nontransgenic mice. *Science* 2012;338(6109):949–953.

736 53. Rey NL et al. Widespread transneuronal propagation of α-synucleinopathy triggered in olfactory
737 bulb mimics prodromal Parkinson's disease. *J Exp Med* 2016;213(9):1759–1778.

738 54. Al-Sadi RM, Ma TY. IL-1beta causes an increase in intestinal epithelial tight junction
739 permeability. *J. Immunol.* 2007;178(7):4641–4649.

740 55. Capaldo CT, Nusrat A. Cytokine regulation of tight junctions. *Biochim Biophys Acta*
741 2009;1788(4):864–871.

742 56. Forsyth CB et al. Increased Intestinal Permeability Correlates with Sigmoid Mucosa alpha-
743 Synuclein Staining and Endotoxin Exposure Markers in Early Parkinson's Disease. *PLOS ONE*
744 2011;6(12):e28032.

745 57. Gray MT, Munoz DG, Gray DA, Schlossmacher MG, Woulfe JM. Alpha-synuclein in the
746 appendiceal mucosa of neurologically intact subjects. *Mov. Disord.* 2014;29(8):991–998.

747 58. Labrie V, Brundin P. Alpha-Synuclein to the Rescue: Immune Cell Recruitment by Alpha-
748 Synuclein during Gastrointestinal Infection. *JIN* 2017;9(5):437–440.

749 59. Kelly LP et al. Progression of Intestinal Permeability Changes and Alpha-Synuclein Expression in
750 a Mouse Model of Parkinson's Disease. *Mov Disord* 2014;29(8):999–1009.

751 60. Haenseler W et al. Excess α-synuclein compromises phagocytosis in iPSC-derived macrophages.
752 *Sci Rep* 2017;7(1):9003.

753 61. Takagawa T et al. An increase in LRRK2 suppresses autophagy and enhances Dectin-1–induced
754 immunity in a mouse model of colitis. *Science Translational Medicine* 2018;10(444):eaan8162.

755 62. Erickson MA, Hansen K, Banks WA. Inflammation-induced dysfunction of the low-density
756 lipoprotein receptor-related protein-1 at the blood-brain barrier: protection by the antioxidant N-
757 acetylcysteine. *Brain Behav. Immun.* 2012;26(7):1085–1094.

758 63. Cardoso FL et al. Exposure to Lipopolysaccharide and/or Unconjugated Bilirubin Impair the
759 Integrity and Function of Brain Microvascular Endothelial Cells. *PLOS ONE* 2012;7(5):e35919.

760 64. Erny D et al. Host microbiota constantly control maturation and function of microglia in the CNS.
761 *Nat. Neurosci.* 2015;18(7):965–977.

762 65. Sampson TR et al. Gut Microbiota Regulate Motor Deficits and Neuroinflammation in a Model of
763 Parkinson's Disease. *Cell* 2016;167(6):1469-1480.e12.

764 66. Chen SG et al. Exposure to the Functional Bacterial Amyloid Protein Curli Enhances Alpha-
765 Synuclein Aggregation in Aged Fischer 344 Rats and *Caenorhabditis elegans*. *Scientific Reports*
766 2016;6:34477.

767 67. Wendeln A-C et al. Innate immune memory in the brain shapes neurological disease hallmarks.
768 *Nature* 2018;556(7701):332–338.

769 68. Steiner JA, Quansah E, Brundin P. The concept of alpha-synuclein as a prion-like protein: ten
770 years after. *Cell Tissue Res.* 2018;373(1):161–173.

771 69. Recasens A et al. Lewy body extracts from Parkinson disease brains trigger α-synuclein pathology
772 and neurodegeneration in mice and monkeys. *Ann. Neurol.* 2014;75(3):351–362.

773 70. Hansen C et al. α-Synuclein propagates from mouse brain to grafted dopaminergic neurons and
774 seeds aggregation in cultured human cells. *J Clin Invest* 2011;121(2):715–725.

775 71. Angot E et al. Alpha-Synuclein Cell-to-Cell Transfer and Seeding in Grafted Dopaminergic
776 Neurons In Vivo. *PLOS ONE* 2012;7(6):e39465.

777 72. Desplats P et al. Inclusion formation and neuronal cell death through neuron-to-neuron
778 transmission of α-synuclein. *Proc Natl Acad Sci U S A* 2009;106(31):13010–13015.

779 73. Sacino AN et al. Intramuscular injection of α-synuclein induces CNS α-synuclein pathology and a
780 rapid-onset motor phenotype in transgenic mice. *Proc Natl Acad Sci U S A* 2014;111(29):10732–
781 10737.

782 74. Uemura N et al. Inoculation of α-synuclein preformed fibrils into the mouse gastrointestinal tract
783 induces Lewy body-like aggregates in the brainstem via the vagus nerve. *Molecular*
784 *Neurodegeneration* 2018;13:21.

785 75. Pan-Montojo F et al. Environmental toxins trigger PD-like progression via increased alpha-
786 synuclein release from enteric neurons in mice. *Sci Rep* 2012;2:898.

787 76. Ulusoy A et al. Neuron-to-neuron α-synuclein propagation in vivo is independent of neuronal
788 injury. *Acta Neuropathol Commun* 2015;3(13):1–13.

789 77. Villumsen M, Aznar S, Pakkenberg B, Jess T, Brudek T. Inflammatory bowel disease increases
790 the risk of Parkinson's disease: a Danish nationwide cohort study 1977-2014. *Gut* 2018;68(1):18–24.

791 78. Fujioka S et al. Occurrence of Crohn's disease with Parkinson's disease. *Parkinsonism & Related*
792 *Disorders* 2017;37:116–117.

793 79. Jung S et al. Analysis of fractalkine receptor CX(3)CR1 function by targeted deletion and green
794 fluorescent protein reporter gene insertion. *Mol. Cell. Biol.* 2000;20(11):4106–4114.

795 80. Kitazawa M, Oddo S, Yamasaki TR, Green KN, LaFerla FM. Lipopolysaccharide-induced
796 inflammation exacerbates tau pathology by a cyclin-dependent kinase 5-mediated pathway in a
797 transgenic model of Alzheimer's disease. *J. Neurosci.* 2005;25(39):8843–8853.

798 81. Schenk M, Bouchon A, Seibold F, Mueller C. TREM-1--expressing intestinal macrophages
799 crucially amplify chronic inflammation in experimental colitis and inflammatory bowel diseases. *J.*
800 *Clin. Invest.* 2007;117(10):3097–3106.

801 82. Grathwohl SA et al. Formation and maintenance of Alzheimer's disease β-amyloid plaques in the
802 absence of microglia. *Nat Neurosci* 2009;12(11):1361–1363.

803 83. Rey NL et al. Spread of aggregates after olfactory bulb injection of α-synuclein fibrils is
804 associated with early neuronal loss and is reduced long term. *Acta Neuropathol* 2017;1–19.

805 84. Schneider CA, Rasband WS, Eliceiri KW. NIH Image to ImageJ: 25 years of image analysis. *Nat.*
806 *Methods* 2012;9(7):671–675.

807

Figures and figure legends

Grathwohl et al., Figure 1

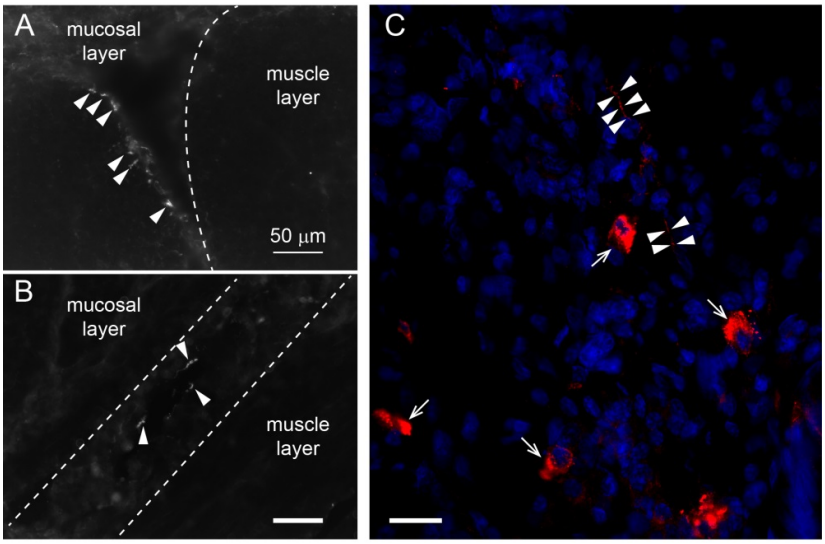

Figure 1

Alpha-Synuclein inclusions in the enteric nervous system and in macrophages of patients with inflammatory bowel disease. (A, B) Immunofluorescence images of αSyn inclusions (Syn1) in the submucosal region of 10 µm cryo-sections from colons of patients with colitis ulcerosa. Arrow heads point to neuritic features indicating presence of inclusions in enteric nerves. Scale bar 50 µm. **(C)** Close-up of a colonic region with active leukocyte infiltration in a patient with ulcerative colitis. Immunoreactivity for αSyn (red) was observed in neuritic features (arrow heads) as well as in individual leukocytes (arrows). Nuclei are shown in blue (DAPI). Scale bar 20 µm.

Grathwohl et al., Figure 2

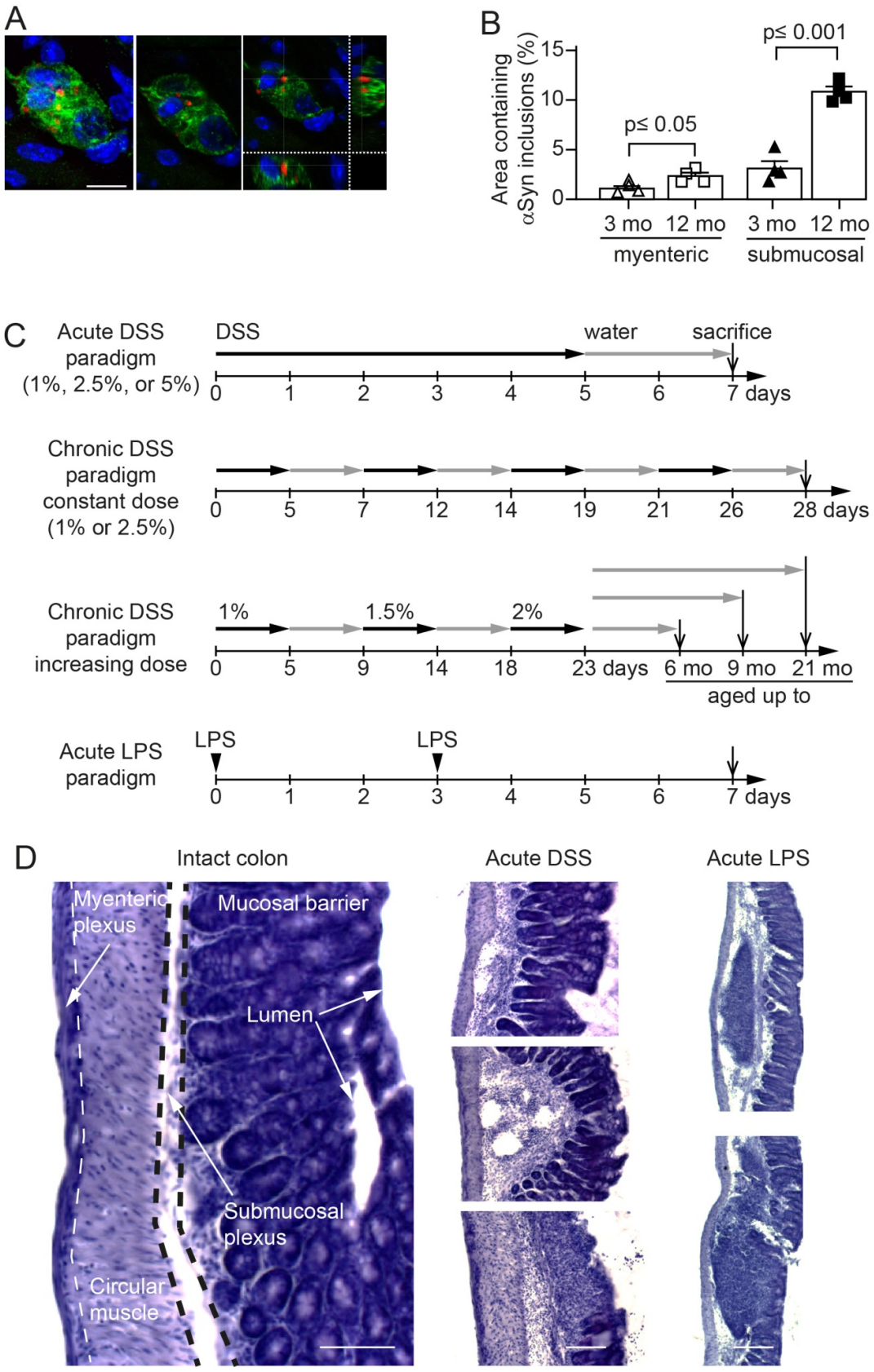

821

Figure 2

Age dependent increase of intracellular αSyn accumulation in enteric nervous system of heterozygous (Thy1)-h[A30P]αSyn transgenic mice and setup of the experimental colitis paradigms. (A) Confocal microscopy imaging of the granular inclusions of human αSyn (red, antibody clone 211) within the ganglia of the submucosal plexus (green, peripherin; blue, DAPI/nuclei) of heterozygous (Thy1)-h[A30P]αSyn transgenic mice. Scale bar, 100 µm. **(B)** Stereological quantification of normally occurring human αSyn inclusions in the myenteric and submucosal plexuses of 3 and 12 months old heterozygous (Thy1)-h[A30P]αSyn transgenic mice (n = 4 per group; mean and S.E.M. are shown; Student t-test between the two age groups in each region). **(C)** Setup of experimental colitis paradigms employing dextran sulfate sodium (DSS, per os in drinking water). Additionally, peripheral inflammation was induced by bacterial lipopolysaccharide (LPS, intraperitoneal injection). After some chronic DSS paradigms mice were aged on normal water up to 6, 9 or 21 months. **(D)** Hematoxylin staining of 35 µm thick colon sections of 3 months old heterozygous (Thy1)-h[A30P]αSyn transgenic mice. Organizational layers of the intact colon (left panel). Representative images of various severity degrees of DSS-driven colitis from weak leukocyte infiltration (top panel of acute DSS) to mucosal ulceration (lowest panel of acute DSS). Note the different appearance of enteric inflammation in acute LPS-driven peripheral inflammation compared with DSS; e.g., confined immune cell clustering and lymphoid hyperplasia; intact mucosal layer. Scale bar 50 µm (intact colon), 100 µm (acute DSS), and 200 µm (LPS).

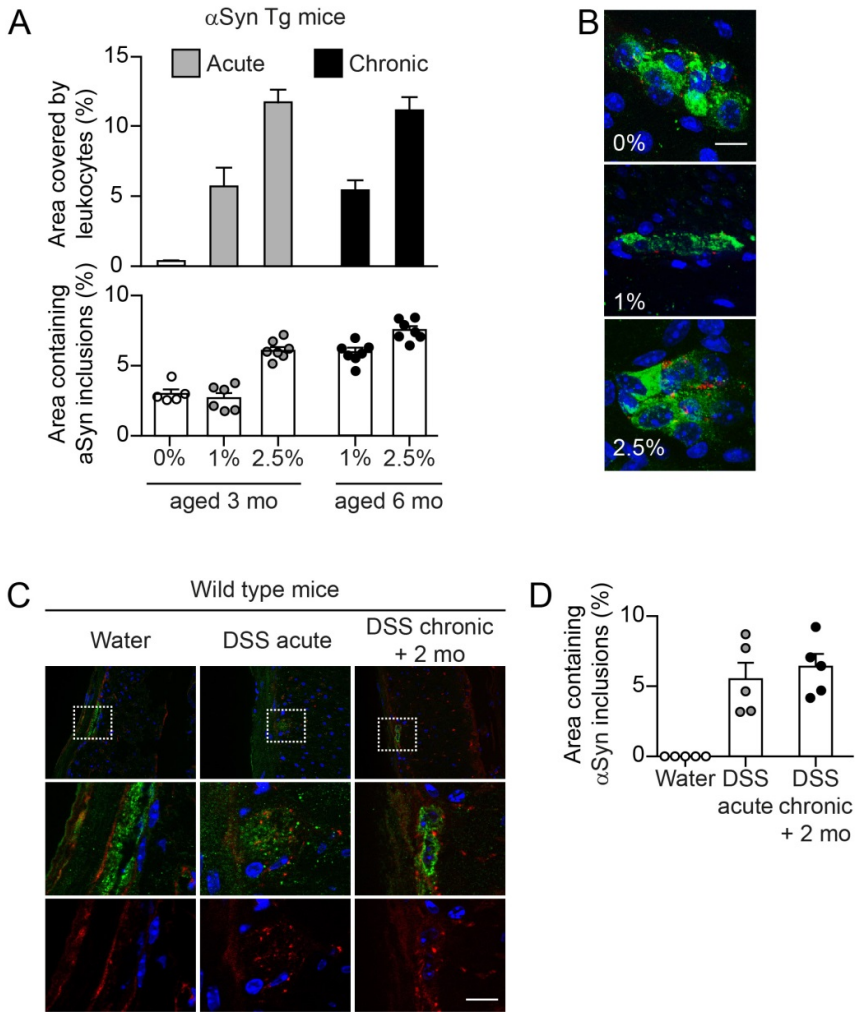

842

843 **Figure 3**

844 **Colitis severity and duration-dependent aggravation of accumulation of αSyn inclusions in the**
845 **colonic submucosal plexus of heterozygous (Thy1)-h[A30P]αSyn transgenic and wild type mice.**
846 **(A)** DSS dose-dependent increase of leukocyte infiltration in the acute and chronic paradigm. The
847 highest acute dose (2.5%) and the two constant chronic doses led to an increase of αSyn inclusions in
848 the submucosal plexus (stereological quantification of αSyn inclusions in the submucosal plexus of 3
849 and 6 months old heterozygous (Thy1)-h[A30P]αSyn transgenic mice (n = 5-7 per group; mean and
850 s.e.m. are shown). **(B)** Representative 2D stacks of confocal images of increasing abundance of αSyn
851 inclusions (red, clone 211 antibody) in a ganglion of the submucosal plexus (green, peripherin) with
852 cellular nuclei in blue (DAPI) n the cute DSS paradigm. Scale bar 200 µm. **(C)** Overview of colonic

region of 3-month-old wildtype mice (top row) exposed to water or acute DSS (5%) with immunofluorescence analysis of murine αSyn load in the colon performed immediately after colitis or exposed to constant chronic DSS (2.5%) and analysis after aging on normal water for another 2 months. White dotted rectangles indicate area that was zoomed out below illustrating in more detail the granular murine αSyn inclusions (red, syn1 antibody) after DSS colitis in the submucosal plexus (green, peripherin antibody). The lower panel shows DAPI and αSyn inclusions without the peripherin channel. Scale bar for the lower two panels 200 µm. **(D)** Stereological quantification of granular murine αSyn inclusions in the submucosal plexus of wildtype mice right after acute DSS colitis or after 2 months of recovery from a 4-week chronic DSS colitis (n = 5 per group). Note the immunoreactivity for the physiological, non-granular αSyn in the enteric nerves of the water group.

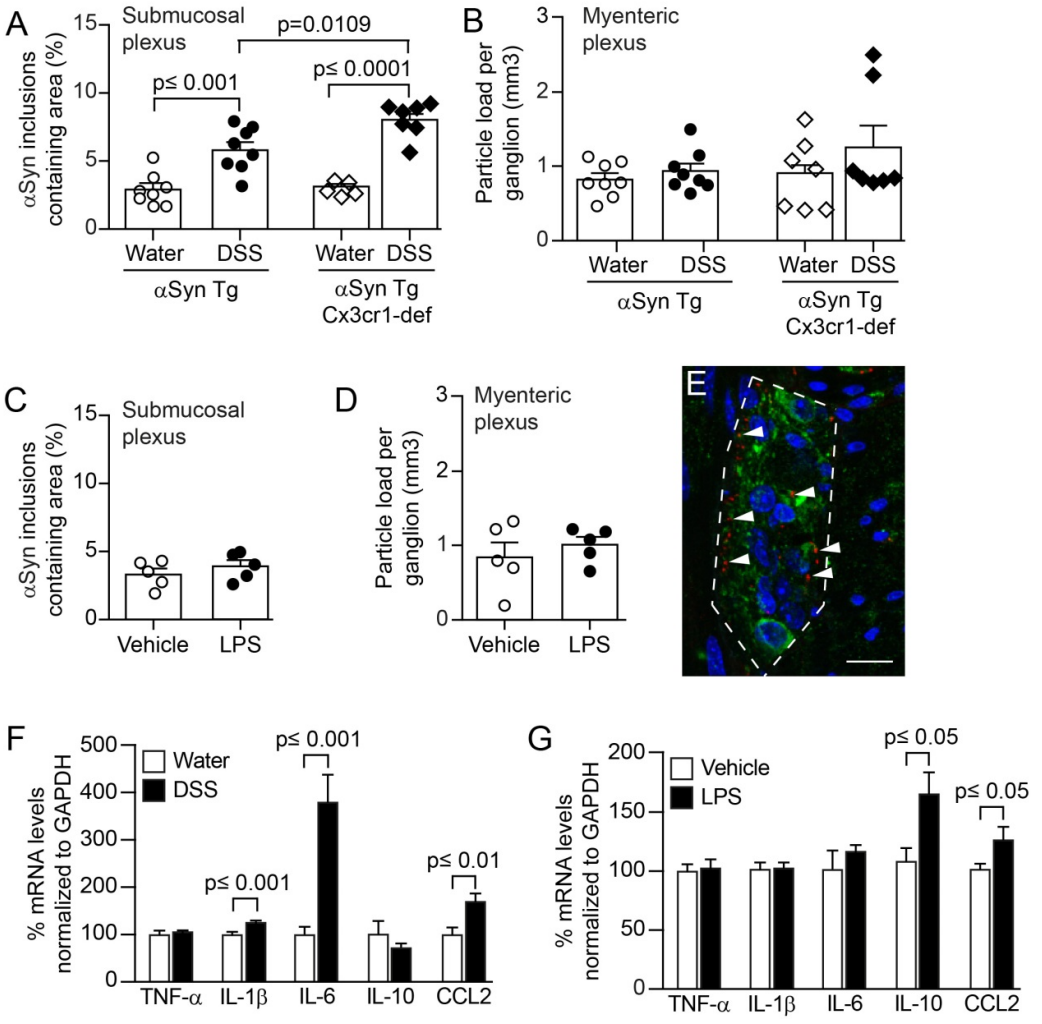

Figure 4

Colitis induced by peroral DSS but not peritoneal LPS enhances αSyn accumulation in the colonic submucosal plexus of heterozygous (Thy1)-h[A30P]αSyn transgenic mice and can be aggravated by lack of Cx3cr1 signaling. Stereological quantification of αSyn inclusions in the submucosal plexus as % area **(A, C)** and in the mucosal plexus as particle load per ganglion **(B, D)** (Two-way ANOVA with Tukey post hoc test). **(E)** Representative 2D stacks of confocal images of intracellular granular αSyn inclusions (red, clone 211 antibody; arrow heads pointing to some selected inclusions) in a ganglion of the myenteric plexus (green, peripherin) with cellular nuclei in blue (DAPI). Scale bar 50 µm. Gene expression analysis of selected cytokines in the colon of (Thy1)-h[A30P]αSyn transgenic mice that received either acutely LPS **(F)** or DSS **(G)** compared to their

877 respective vehicle or water controls. Note the strong increase in IL-6 and the lack of elevation of IL-
878 10 in the DSS paradigm compared to the LPS paradigm indicating a different inflammatory colonic
879 milieu despite the abundant leukocyte infiltration in both paradigms. n = 5-8 per group; mean and
880 s.e.m.; Student's t-test between inflammatory agent and vehicle for individual cytokines.
881

Grathwohl et al., Figure 5

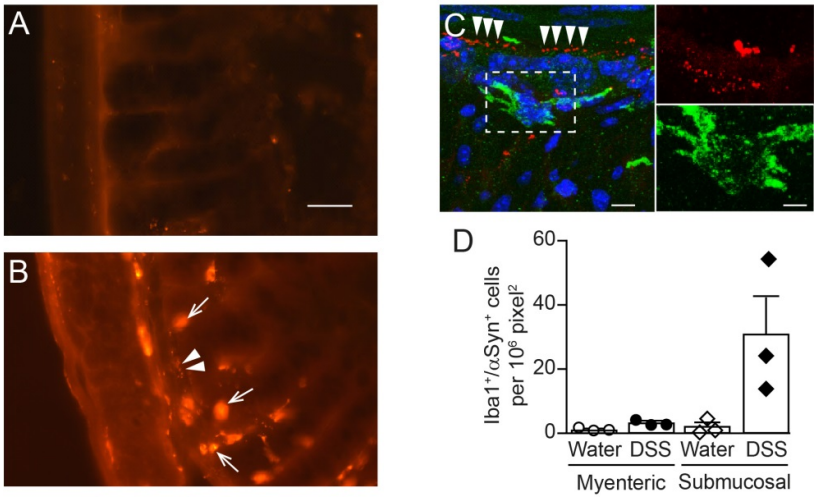

882
883 **Figure 5**
884 **Alpha-synuclein co-localizes with ENS and macrophages upon DSS colitis in αSyn transgenic**
885 **mice. (A, B)** Immunofluorescence image of αSyn staining in colonic region of (Thy1)-h[A30P]αSyn
886 transgenic mice on water **(A)** or after acute DSS colitis (2.5%) **(B)**. Note the small dotted structures of
887 the typical αSyn inclusions in the submucosal plexus (arrow heads) and the large features of
888 immunoreactivity which localize to apparent infiltrating leukocytes (arrows), similar to what was
889 observed in IBD patients in Figure 1. Scale bar 100 µm. **(C)** 2D stacks and close-up of confocal
890 images co-localizing αSyn (red) with the macrophage marker Iba-1 (green) in the colon of a (Thy1)-
891 h[A30P]αSyn transgenic mouse after DSS colitis. Note the dotted structures of the typical αSyn
892 inclusions in the submucosal plexus (arrow heads). Scale bar 40 µm and 13 µm for the close-up. **(D)**
893 Quantification of numbers of Iba-1/αSyn-double positive macrophages (n = 3 per group; mean and
894 S.E.M.)
895

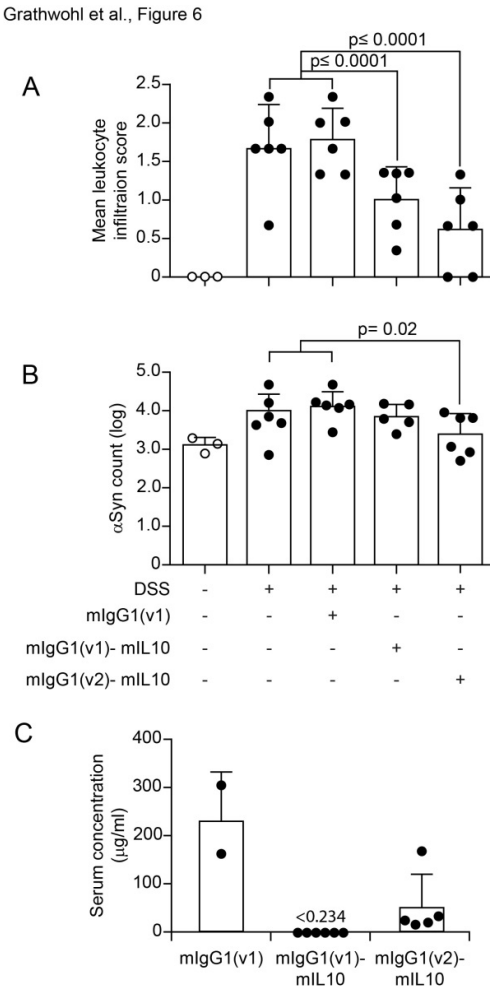

Figure 6

Systemic IL-10 ameliorates DSS colitis and associated local αSyn accumulation in (Thy1)-h[A30P]αSyn transgenic mice. Two different recombinantly engineered and murine IgG1-fused forms of murine IL-10 (mIgG1(v1)-mIL10 and mIgG1(v2)-mIL10) were administered i .p. in an acute DSS paradigm (5%) with (Thy1)-h[A30P]αSyn transgenic mice. Vehicle and the mIgG1(v1) alone served as untreated controls. **(A)** Leukocyte infiltration was assessed by visual scoring and **(B)** inclusion features of αSyn were stereologically and semi-automatically quantified and result log scaled for statistical analysis. Both the vehicle group and the mIgG1(v1) group had similar levels of leukocyte infiltration and αSyn inclusions and were merged for the statistical analysis to compare with the IL-10 treated groups. Both forms of IL-10 ameliorated leukocyte infiltration whereas mIgG1(v2)-mIL10 also blocked the appearance of αSyn inclusions significantly (n = 3-6 per group; mean and

908 s.e.m.; one-way ANOVA and Tukey post hoc test). **(C)** Persistent exposure mIgG1(v2)-mIL10 versus
909 mIgG1(v1)-mIL10 (lower limit of detection is indicated at <0.234) as measured in serum at the end of
910 the in vivo phase corresponds with beneficial treatment effects on αSyn readout observed above. The
911 mIgG1(v1) was only measured in two mice.
912

Grathwohl et al., Figure 7

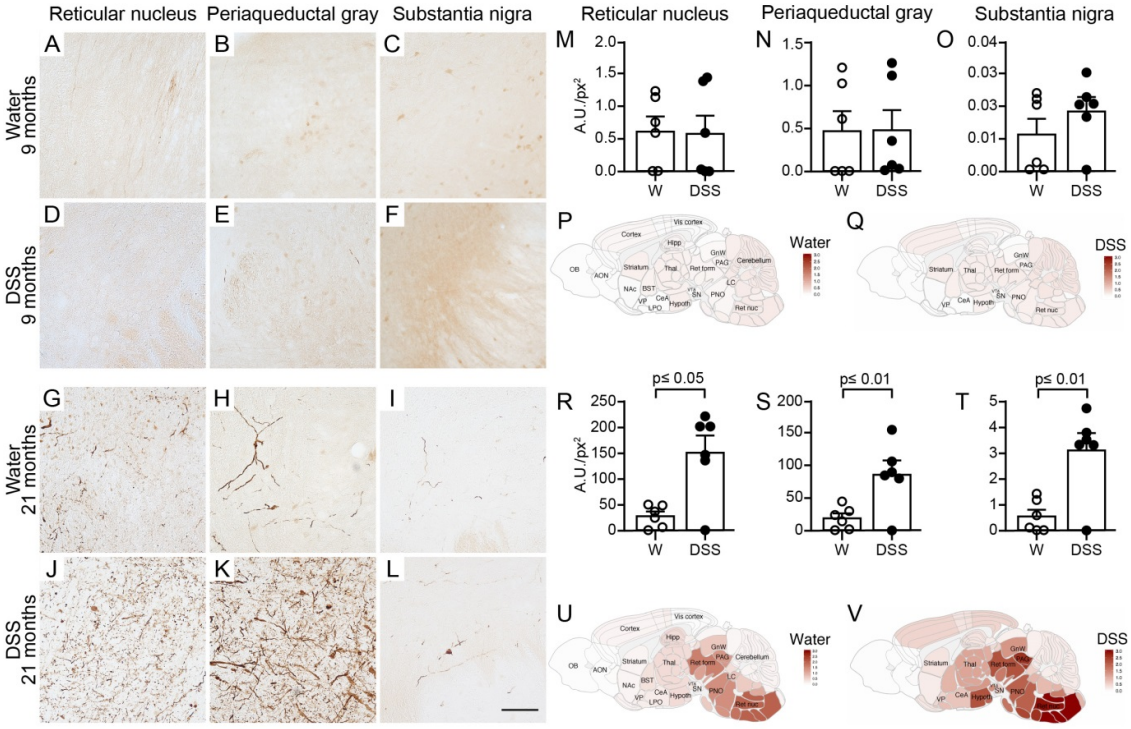

913
914 **Figure 7**
915 **A single chronic DSS colitis insult causes an age-dependent accumulation of proteinase K**
916 **resistant pSer129-αSyn in various brain regions of (Thy1)-h[A30P]αSyn transgenic mice.** A 3-
917 week chronic increasing dose DSS paradigm was performed with 3-month old (Thy1)-h[A30P]αSyn
918 transgenic mice. After recovering and further aging, various brain regions were analyzed for
919 proteinase K resistant pSer129-αSyn immunoreactivity in 9-month **(A-F)** and 21-month old **(G-L)**
920 mice, respectively. Densitometric quantification of pSer129-αSyn immunoreactivity in different brain
921 regions in 9-month **(M-O)** and 21-month old mice **(R-T)** (n=6 mice per group). Statistical analyses
922 were performed using negative-binomial mixed-effects models adjusting for multiple comparisons.

923 Representative heatmap of the average distribution scores of pSer129-αSyn immunoreactivity for
924 each treatment group in varying brain regions in all the 9-month **(P-Q)** and 21-month old **(U-V)** mice
925 was generated in a sagittal mouse brain (n=10 mice per group). Scale bars: 500 µm.
926
927

Grathwohl et al., Figure 8

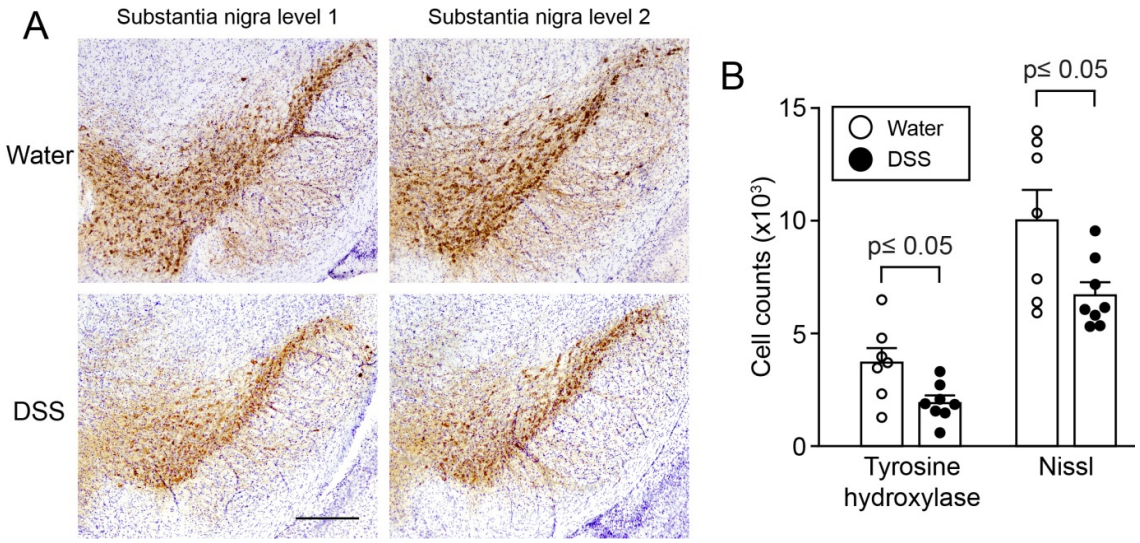

928

929 **Figure 8**

930 L**oss of tyrosine hydroxylase and Nissl positive cells in the substantia nigra of (Thy1)-**
931 **h[A30P]αSyn transgenic mice at 21 months of age, 18 months post recovery from DSS colitis.**
932 (Thy1)-h[A30P]αSyn transgenic mice that were exposed to a chronic DSS-colitis paradigm at 3
933 months and were aged to 21 months showed a significant loss of mean count of cells with tyrosine
934 hydroxylase (TH) immunoreactivity and cellular Nissl staining in the substantia nigra compared to
935 age-matched littermate mice in the group that did not experience DSS colitis (water). **(A)**
936 Representative images of two levels of the substantia nigra in one mouse per group. **(B)** Stereological
937 quantification of cells positive for TH or Nissl (n=7-8 mice per group). Statistical analyses of the TH
938 dataset were performed using Student's T-test, while Welch's T-test was used for the Nissl dataset to
939 adjust for unequal variances. Scale bar: 500 µm.
940